

Sea Spikes and Radar False Alarm Rates

K. D. Ward, R. J. A. Tough, P. W. Shepherd
TW Research Ltd, Harcourt Barn,
Harcourt Road, Malvern, WR14 4DW

Abstract

Progress made in the modelling of spiky sea clutter is reviewed. Controlled data analysis and detailed EM scattering calculations can now make direct contact with the GIT and RRE empirical clutter models and the K distribution. Problems encountered in modelling the effects of imperfect frequency agility are discussed; their solution has yielded a robust, versatile and well-characterised tool for radar performance assessment. The scan-to-scan CFAR processing developed earlier in this project has been improved, and its performance assessed in more detail.

Keywords: Radar, Sea clutter, sea spikes, target detection

Introduction

The detection of small targets in a maritime environment is hampered by unavoidable radar returns from the sea. To overcome this difficulty we must characterise the clutter in sufficient detail to distinguish and exploit the ways in which it differs from the expected target returns. Simple Gaussian statistical models provide a framework for this analysis in the case of low-resolution radar systems and suggest useful target detection strategies. High-resolution maritime radars are able, in effect, to image some of the structure of the sea surface and consequently are plagued by spiky non-Gaussian clutter. Gaussian based detection methods no longer work well in this context. To overcome these problems, the K distribution has been developed, and applied successfully to small maritime target detection [1]. Its motivation and justification have nonetheless been in the main empirical, and relatively little contact has been made with the more detailed description of the scattering of microwaves by the sea surface.

In this project we have developed methods for calculating low grazing angle scattering by an imperfectly conducting surface and used these, in conjunction with models for the sea surface height fluctuations, to characterise the properties of sea clutter. We reproduced the dependence of the mean clutter RCS on polarisation, grazing angle and sea state captured by the Georgia Tech clutter model [2] and made satisfactory contact with an empirical characterisation of the single point fluctuations in the clutter [3]. However, attempts to extend this model to the description of the correlation properties of the clutter, which can be used to differentiate it from target returns, revealed that the model was not able to reproduce their behaviour over time-scales relevant to small target detection. Most pertinently, the transiently coherent spatial structure observed in the clutter, which impacts significantly on detection performance, is not contained in the sea surface models, which are derived from extensively averaged data. Nonetheless it was possible to model the evolution of this transient structure, by incorporating the dispersive behaviour of sea surface waves, and so construct a useful scan-to-scan

CFAR detector [4], whose performance is up to 10 dB better than that of conventional CFAR processing [4,5].

This paper reviews some of the progress made in the final year of the project, during which several outstanding problems in the modelling of LGA EM scattering have been resolved, the scan-to-scan CFAR has been developed further and its performance has been assessed in more detail.

Scattering calculations and empirical clutter models

In our earlier work [3] we described how Holliday's Forward Back (FB) method of calculating VV scattering by a perfectly conducting surface could be modified to introduce effects of imperfect conductivity through the incorporation of an impedance boundary condition (IBC). This analysis has now been extended to HH scattering. For Hpol, the IBC introduces a spurious divergent contribution to the kernel of the scattering integral equation whose effects must be removed by a suitable regularisation; this apparent divergence must also be taken account of when calculating the adjunct plane terms required to remove unwanted finite size effects from the results. We now have an efficient scattering code, which we have used in a detailed analysis of the physical origin of observed sea clutter characteristics. This has shown that contributions from the scattering by small-scale structure, modulated by the sea swell, and from breaking waves, are sufficient to account for the average Radar Cross Section (RCS) and the VV/HH differences observed in practice. Close to grazing incidence, multipath and shadowing are important; our detailed calculations have validated Katzin's [6] analysis of these effects, which we have incorporated into our model. The output from this is in good agreement with the GIT results [2].

To assess further the validity of these models we have analysed airborne radar clutter measurements, and looked at the variation of characteristics with grazing angle, as the aircraft approaches a defined area of sea, at a fixed altitude. This analysis has provided further validation of our physical model for the average RCS at low grazing angles. However, the variations with grazing angle of the clutter data fluctuation properties (manifest in the K distribution shape parameter, ν) do not agree well with either the predictions of the physical model or the existing average empirical formula [8]. Consequently much remains to be done in the detailed characterisation of sea clutter; we feel that our combination of controlled data analysis and a priori scattering calculation will continue to provide useful tools in this study.

Modelling imperfect frequency agility

To achieve effective de-correlation of the speckle component of clutter, the radar agile frequency must step by the pulse bandwidth, at the very least. (If the clutter is not homogeneous within the resolution cell, a larger step is required). Consequently there can be more pulses in the beam dwell time than there are available independent agile frequencies. Thus, after pulse-to-pulse integration, the numbers of available independent clutter and noise samples can be different. This rather subtle effect, which has an impact on radar performance and our understanding of the mechanisms involved, can be incorporated into our compound K modelling as follows.

The intensity of a coherent signal of amplitude a , embedded in a complex Gaussian process, which can represent the sum of clutter and thermal noise contributions, has a Ricean pdf; the effect of non-Gaussian clutter characteristics can be introduced by assigning it a gamma distribution of local power.

$$P(z|x, a, n) = \frac{1}{x+n} \exp\left(-\frac{a^2+z}{x+n}\right) I_0\left(\frac{2a\sqrt{z}}{x+n}\right) \quad (1)$$

$$P(x) = \frac{b^\nu}{\Gamma(\nu)} x^{\nu-1} \exp(-bx)$$

Here I_L is a modified Bessel function of the first kind, and of order L . When we have equal numbers N of independent samples of thermal noise and clutter, i.e. for perfect frequency agility, the effect of integration over these samples is captured by

$$Z = \sum_{k=1}^N z_k, A^2 = \sum_{k=1}^N a_k^2$$

$$P(Z|x, A, n, N) = \left(\frac{Z}{A^2}\right)^{\frac{N-1}{2}} \exp\left(-\frac{Z+A^2}{x+n}\right) \times \quad (2)$$

$$I_{N-1}\left(\frac{2A\sqrt{Z}}{x+n}\right)$$

As Shnidman [8] has stressed, the whole range of Swerling target models can be introduced into the analysis by assigning appropriate gamma distributions to the amplitudes a ; this author also discusses effective numerical methods for performing the required integration over these pdfs in noise alone. In the case where we have different numbers of independent samples of clutter and noise, however, his analysis is not applicable. By incorporating the clutter signal into the amplitude a , and at the expense of introducing a further integration over the appropriate Rice distribution of this quantity, we have overcome these difficulties. The evaluation of the nested integrations that arise in this approach can be made very efficient by exploiting the properties of the modified Bessel and hypergeometric functions; the accuracy of these calculations is also easy to control. This provides us with a robust and versatile tool with which to analyse the interaction between imperfect frequency agility and radar performance. An illustration of the effect on false alarm rate is shown in Figures 1 and 2. Figure 1 shows the

probability of false alarm (P_{FA}) versus threshold for the sum of 10 pulses of K clutter plus noise (CNR= 0dB); the different curves correspond to K distribution shape parameters ν (100, 30, 10, 3, 1, 0.3, 0.1) and it is assumed that there are 10 independent samples of clutter speckle and noise. Figure 2 takes the right-most curve, $\nu=0.1$, and shows the effect of reducing the number of independent speckle samples. There is a significant effect of the imperfect frequency agility on P_{FA} , which should be modelled to give accurate performance estimation.

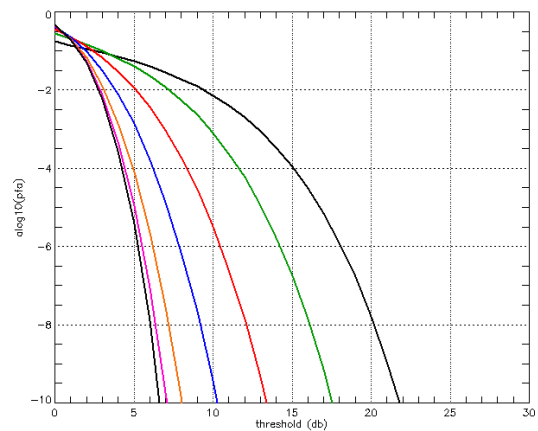


Figure 1: Variation in P_{FA} with threshold; 10 pulses averaged and $\nu=100,30,10,3,1,0.3,0.1$. See text for details.

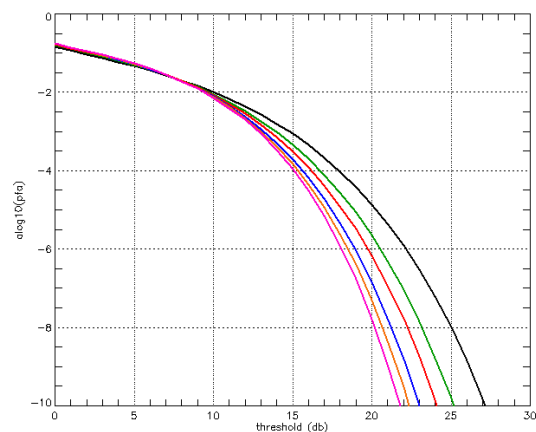


Figure 2: Variation in P_{FA} with threshold; $\nu=0.1$, 10 pulses averaged with 1,2,3,5,7 and 10 independent samples of clutter speckle. See text for details

Scan-to-scan CFAR

Conventional cell averaging CFAR (constant false alarm rate) systems set a detection threshold on each test cell that is proportional to the mean of surrounding range and azimuth cells. By using the spatially correlated structure of sea clutter, it may be possible improve performance by predicting the mean level of the test cell from the surrounding data by more sophisticated means than just the local average. As we discussed in [4], attempts to do this using surrounding range and azimuth cells from a single radar scan have been frustrated by the apparent non-stationarity manifest in sea clutter data (referred to as transient coherence). Thus, we have extended the process to use radar scans before and after the scan under test, thereby allowing the CFAR to set the threshold using only data very close to the cell under test.

Figure 3 shows a typical range-time-intensity (RTI) plot of sea clutter (with 512 range samples at 0.3m spacing in the horizontal dimension, and 512 time samples at half second intervals in the vertical direction); the data is vertically polarised, and measured from a cliff-top radar. Figure 4 is the 2D Fourier transform of figure 3, and shows a bright line corresponding to the dispersion relation between frequency ω , wave number k and tidal current velocity along the line of sight v

$$\omega = \omega(k) = kv \pm \sqrt{kg}, \quad (3)$$

for waves travelling towards the radar. There are also harmonics of this main dispersion line and a fainter line for waves travelling away from the radar. If we consider just the main waves approaching the radar, equation (3) allows us to describe the temporal evolution of a Fourier component of a range profile quite simply. We denote the range profile intensity at range r and time t by $R(r;t)$; its Fourier

transform can then be represented formally by

$$\tilde{R}(k;t) = \int \exp(ikr)R(r;t) \quad (4)$$

The corresponding value of the Fourier component with wave number k , now measured at time $t + \Delta t$, is given by

$$\tilde{R}(k;t + \Delta t) = \tilde{R}(k;t)\exp(+i\omega(k)\Delta t) \quad (5)$$

which incorporates the dispersion relation (3) explicitly. Thus range profile at $t + \Delta t$ can be retrieved by Fourier inversion as

$$R(r;t + \Delta t) = \frac{1}{2\pi} \int \exp(-ikr + i\omega(k)\Delta t)\tilde{R}(k;t)dk \quad (6)$$

Consequently the clutter component in the range profile at time $t + \Delta t$ can be estimated from that at time t . In practice a small number (n) of range profiles, measured before and after the test profile, are analysed in this way. Each gives an estimate of the clutter level in the test profile; these can then be averaged to provide an improved estimate. Figure 5 shows the clutter values estimated from figure 3 using $n=3$ (the unknown tidal current v is derived by minimising the standard deviation of the difference between Figures 3 and 5). Any target or debris returns will tend to smear out when propagated through (6), which is specifically designed to retain the coherent structure of sea surface features.

The estimate derived from the surrounding scans may now be used to threshold the test cell. Figure 6 compares P_D versus P_{FA} for this process (left curve) with a conventional CA-CFAR using a long term average for the threshold (right curve) and a signal to clutter ratio (SCR) of 5dB. Clearly the scan-to-scan CFAR has superior performance. Repeating these calculations at different values of SCR shows that, for this data, the improvement is 4.8 dB for a non-fluctuating target, $P_D=0.5$ and $P_{FA}=10^{-4}$.

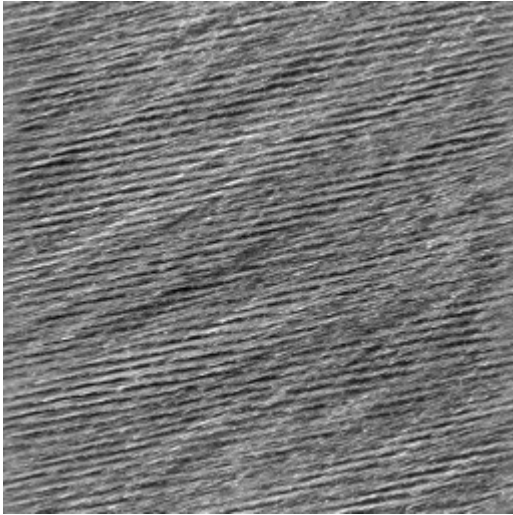


Figure 3: Range Time Intensity plot of MDC613

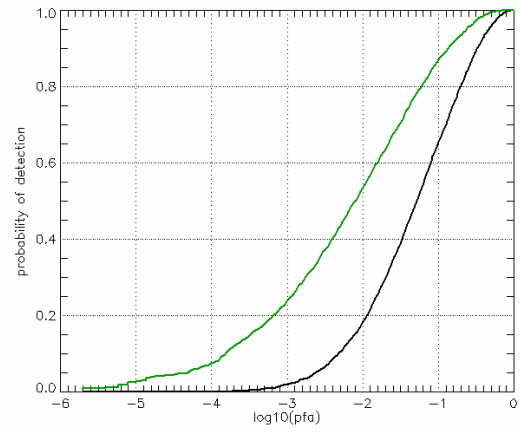


Figure 6: MDC 613 P_D vs. P_{FA} for fixed threshold (left curve) and scan-to-scan CFAR (right curve); signal to clutter ratio 5 dB

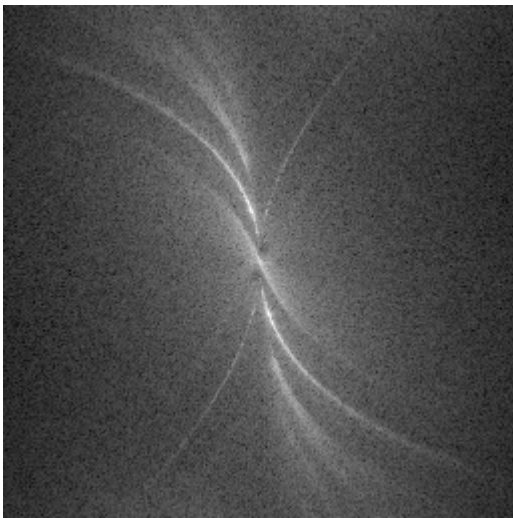


Figure 4: ω - k plot of MDC613

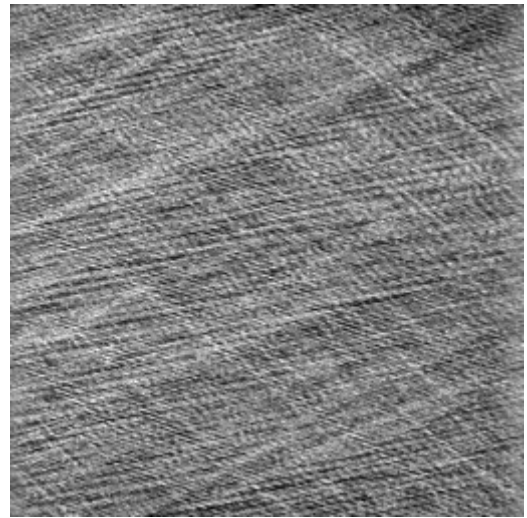


Figure 7: Range Time Intensity plot of MDC610

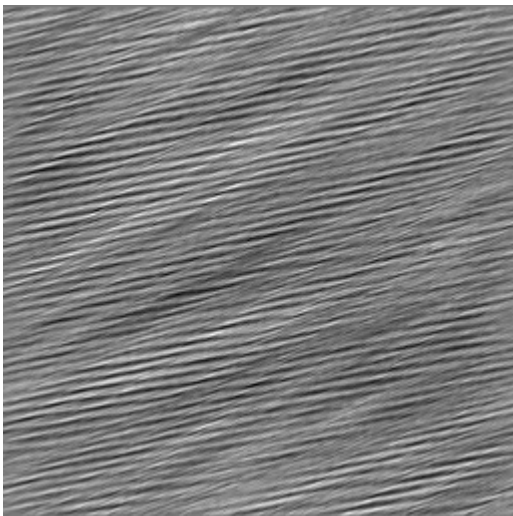


Figure 5: CFAR estimate for MDC613

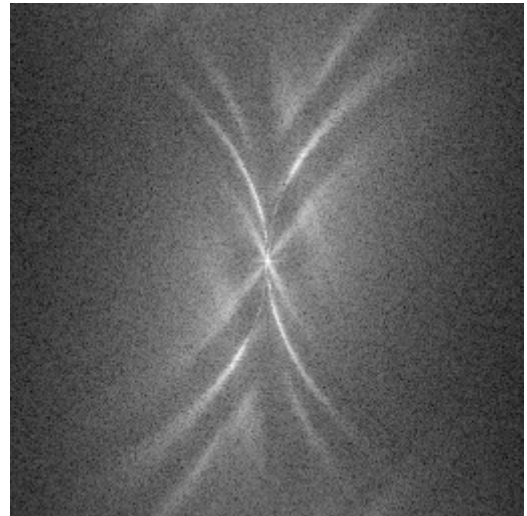


Figure 8: ω - k plot of MDC610

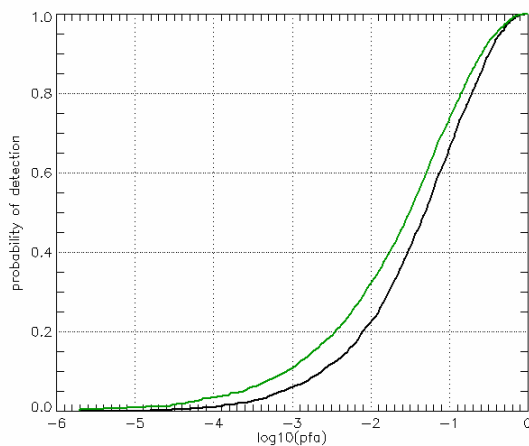


Figure 9: MDC 610 P_D vs. P_{FA} for fixed threshold (left curve) and scan-to-scan CFAR (right curve); signal to clutter ratio 5 dB

Figures 7, 8 and 9 show a more challenging, and less common, condition where there is significant wave energy in both directions (towards and away from the radar). Thus the ω - k plot in figure 8 has two bright dispersion lines. Even in this situation, if we choose to predict using the advancing waves, we obtain an improvement (albeit smaller than before) over conventional CFAR, as shown in Figure 9. Again, repeating these calculations at different values of SCR shows that the improvement is 1.1 dB for a non-fluctuating target, $P_D=0.5$ and $P_{FA}=10^{-4}$.

Many more cases have been analysed, and generally show an improvement using scan-to-scan CFAR. The best results tend to be obtained with Vertical polarisation, where the wave structure is most evident in the RTI plots. With Horizontal polarisation there are often large spikes, which tend to obscure the correlated wave structure and cause errors in the predictions. It is also interesting to consider the effects of radar resolution and scan rate. Here, the best performance improvements are obtained with either high range resolution and a fast scan rate, or lower range resolution and a slow scan rate. This seems to be associated with the faster decorrelation of short waves than of long waves. A high-resolution radar

resolves the short waves and needs a fast scan to exploit them; if not they appear as noise and reduce performance.

Conclusions

EM Scattering calculations from realistic sea surface simulations have reproduced average experimental clutter RCS trends at low grazing angles. New methods for calculating radar performance in sea clutter have been developed. A new scan-to-scan CFAR, with superior performance to conventional methods, has been demonstrated on recorded sea clutter data.

References

1. Ward, KD, Tough, RJA and Watts, S, 'Sea Clutter: Scattering, the K Distribution and Radar Performance', IEE Publishing, 2006
2. Horst, MM, Dyer, FB, and Tuley, MT, 1978, Int. IEEE AP/S URSI Symposium, Maryland, 6-10
3. Tough, RJA, Ward, KD, Shepherd, PW, Paper A2, 1st EMRS DTC Technical Conference, Edinburgh, 2004
4. Tough, RJA, Ward, KD, Shepherd, PW, Paper A2, 2nd EMRS DTC Technical Conference, Edinburgh, 2005
5. Tough, RJA, Ward, KD, Shepherd, PW, EuRAD01: Selected Radar Topics from EMRS DTC, Paris, 2006
6. Katzin, M, Proc. IRE, **45**, 44-54, 1957
7. Ward, KD, Baker, CJ, and Watts, S, IEE Proc. F, **137**, 51, 1990,
8. Shnidman, D, IEEE Trans., **AES-39**, 1059-68, 2003, and references therein.

Acknowledgements

The work reported in this paper was funded by the Electro-Magnetic Remote Sensing (EMRS) Defence Technology Centre, established by the UK Ministry of Defence and run by a consortium of Selex Sensors & Airborne Systems, Thales Defence, Roke Manor Research and Filtronic.